



# CHARACTERIZATION TECHNIQUE TO EVALUATE THE PROPERTIES OF NANO-STRUCTURES

Upendra Sharan Gupta<sup>1</sup>, Rahul Singh<sup>2</sup>, Savan Parmar<sup>3</sup>, Prasanna Gupta<sup>4</sup>

<sup>1</sup> Reader, <sup>2,3,4</sup>UG Scholar, Dept. of Mech. Engineering, SVITS, Indore, (India)

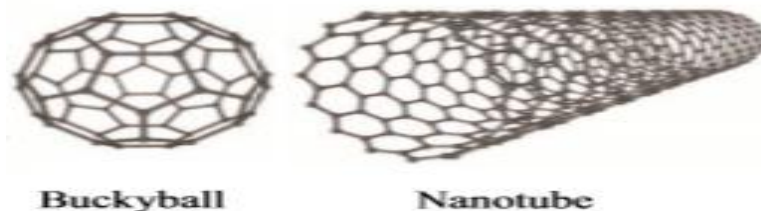
## ABSTRACT

*In this paper, the experimental methods used to characterize the thin films and nanostructures are summarized and explained. These methods include various imaging modes of electron microscopy, x-ray diffraction and magnetic characterization techniques, etc. From the information delivered by these methods, the morphology, elemental composition, phase transitions, crystallinity, optical properties and magnetic properties of the samples can be determined.*

**Keywords:** Nano tribology, Nano structure, carbon nanotube.

## I. INTRODUCTION TO NANOSTRUCTURED MATERIALS

Nanostructures usually refer to structured devices with a size of few nanometers to several hundreds of nanometers. E.g. cell components or viruses, extremely small sand grains or nonmetric droplets of water. Nanostructures are further classified into inorganic nanostructures and organic nanostructures [1]. **Inorganic nanostructures:** A well-known group of inorganic nanostructures is the fullerenes. They are part of the allotropes of the carbon, one of the most important elements in nature. The fullerenes [2] introduced new stable carbon structures in the form of hollow spheres called Bucky balls or buckminsterfullerene, onion-like graphitic sphere tubes called carbon nanotubes [3]. **Nanotubes** find their application in a wide range of techniques such as components of Nano electronic devices like field-effect transistors, and are also good components for mechanically reinforced composite materials and nanometer sized sensors.



The potential of applications of the nanotubes led to the development of other kinds of small cylindrical shaped Nano-objects: the **nanowires** (also called **Nano rods**). These Nano objects, essentially based on metallic elements, are wire-like nanomaterials, such as carbides[4], nitrides[5], oxides[6,7], having as common characteristic a cylindrical symmetric cross-section.



Fig. 1 Example of nanowires: (a) and (b) are hexagon and pentagon shaped ZnO nanowires, whereas (c) presents GaN nanowires.

## 1.1 Organic Nanostructures

The organic nanostructures are chemical compounds consisting primarily of carbon and hydrogen. They are extremely flexible in being tailored to meet the needs of particular applications. They show great potential for coating and molding as well as their production cost is also low. Nanostructured organic thin films are used as organic light emitting devices (OLEDs) and also as organic thin film transistors [8, 9, 10].

## II. CHARACTERIZATION TECHNIQUES

### 2.1.1 Transmission Electron Microscopy (TEM)

Transmission electron microscopy (TEM) is the main technique used to resolve the structure and crystallinity of nanomaterials. . Both the imaging mode and the diffraction mode can be applied, depending on the pathway of electrons, which can be controlled by the arrangement and settings of apertures and lenses.

In a TEM instrument, a high-speed electron beam hits a sample that is thin enough (normally about 10 to 100 nm) that electrons can pass through and be captured by a CCD camera. In common TEM imaging, sub-nanometer resolution can be reached. With high-resolution TEM (HRTEM), the magnification is larger so that atomic distances can be resolved, but this normally requires the help of model systems and simulation of the electron-beam phase contrast [11]. The common mode of TEM is the bright-field (BF) imaging mode, where the (000) transmitted beam contributes to the image. In this mode, image contrast arises from occlusion and absorption of electrons in the sample. Thicker regions or regions with a higher atomic number will appear darker than other regions, due to stronger scattering and absorption of the electrons. In the dark-field (DF) imaging mode, the (000) beam is excluded, and diffraction contrast contributes solely to the image. Therefore, DF configuration is normally used for low-resolution purposes, but with a clear contrast indicating different crystal orientations, grain boundaries and defects[11].

In the diffraction mode, Bragg diffractions are expected because the electrons have a well-defined wavelength. When hitting a crystalline specimen, the incident electron wave will interact with the crystal lattice; as a result, electrons are scattered by certain crystal planes. By measuring the selected area electron diffraction (SAED) pattern, crystallographic characteristics, such as lattice parameter and symmetry, can be determined with high precision.

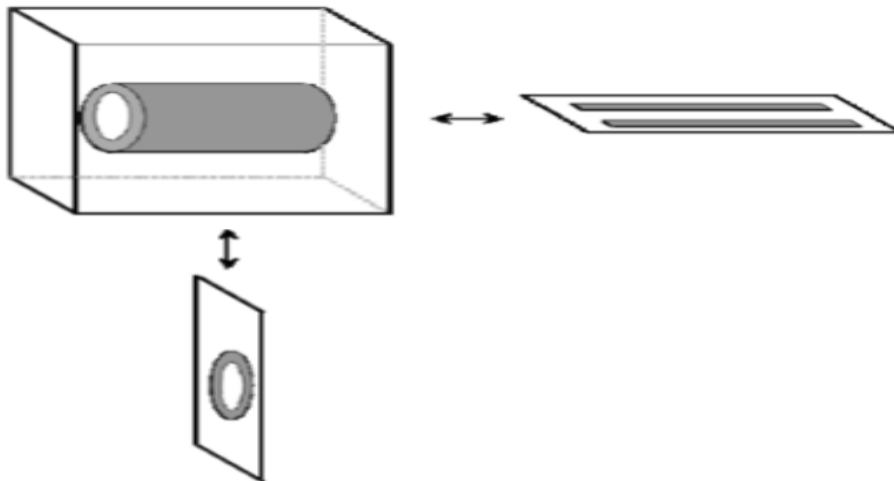


**Fig 2: Two-dimensional slices taken through a 3D reconstruction of a tomographic scan. The locations of the section can be chosen arbitrarily.**

### 2.1.2 Electron Tomography

Three-dimensional (3D) structures of nanotubes were resolved with the help of electron tomography (ET). Unlike the well-known CT technique used in medical care, which utilizes x-rays to penetrate the sample and generate projection images, ET makes use of electrons in the TEM device. The basic principle of tomography is shown in Figure 2. A 3D object can be reconstructed from 2D projections in different directions, which can then be examined along arbitrarily chosen planes (sections). Besides electrons and x-rays,  $\gamma$ -rays and ions can also be used for tomographic imaging. Due to the advantage of the ability to focus electrons into a small beam, the combination of ET with an existing TEM is an ideal tool for 3D structure determination of nanomaterials with high spatial resolution [12]. In TEM, both BF and DF operation modes are possible for ET. The use of BF TEM for tomography is often affected by Bragg contributions, which makes it very difficult to interpret the phase-dominated contrast [12]. However, combining DF STEM mode with a HAADF detector can be used to avoid Bragg contributions. In this technique, a high angle annular aperture excludes the central beam and all electrons scattered up to a certain angle from imaging; thus, a mass-thickness contrast is generated that depends exponentially on sample thickness.

### 2.1.3 Scanning Electron Microscopy (SEM)

The scanning electron microscope (SEM) is a type of electron microscope capable of producing high-resolution images of a sample surface. A sketch of the electron beam path is shown in Figure 3. SEM can have several imaging modes, such as secondary electron mode, back-scattered electron mode, Auger electron mode, x-ray analytic mode, and so on [13]. The spatial resolution of SEM depends on the size of the electron spot. In advanced systems, a field-emission (FE) gun is used to produce sharp electron beams with high current and high coherency, thus achieving much higher magnification with better image quality. Because the incoming beam interacts with a much bigger sample volume—from several hundreds of nanometers up to micrometers—compared to the distances between atoms, and different from TEM, the information are obtained from secondary electrons or backscattered electrons from the whole information volume, the resolution of SEM is not high enough to reach the atomic scale. The highest spatial resolution of a FE-SEM is typically 1 nm – 20 nm,

depending on the individual instrument and properties of the sample itself. However, SEM has compensating advantages, including the ability to quickly image a comparatively large area of the specimen and simple sample preparation procedures.

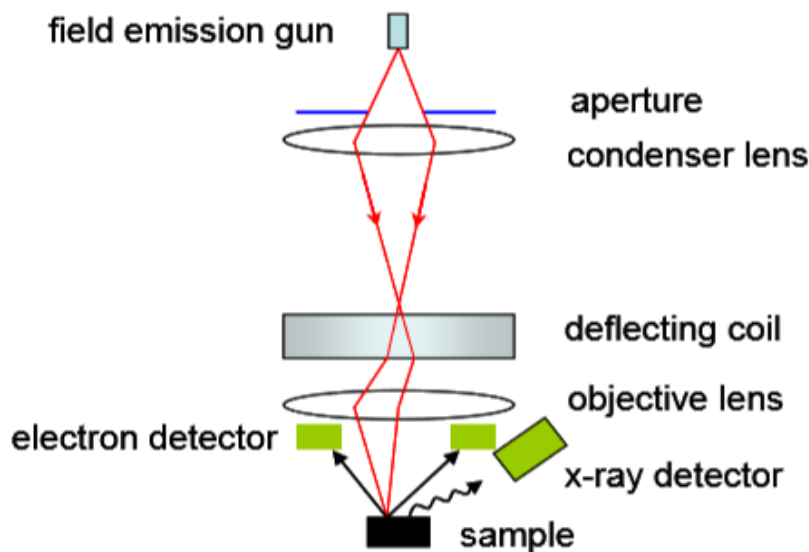
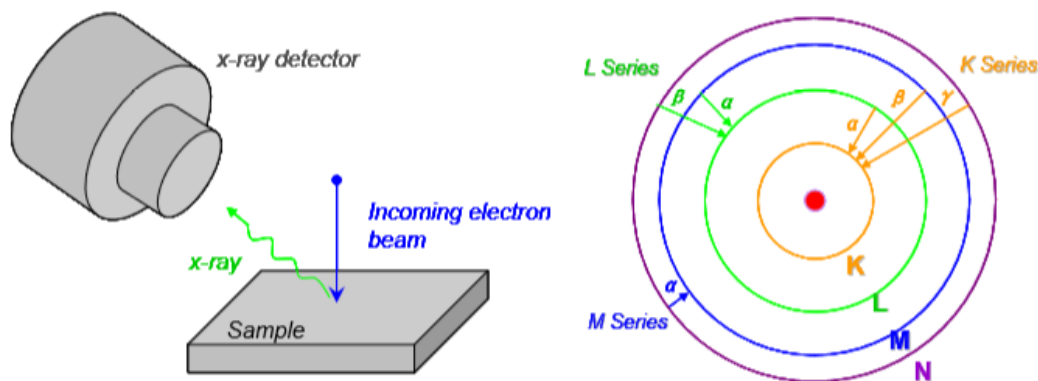


Fig 3: Schematic view of a scanning electron microscope (SEM).

#### 2.1.4 Energy-Dispersive X-Ray Spectroscopy (EDX)

Energy-dispersive x-ray spectroscopy (EDX or EDS) is a method used to determine the energy spectrum of x-ray radiation. It is a technique used for identifying the elemental composition of a specimen. During EDX analysis, the specimen is bombarded with an electron beam inside an SEM. The bombarding electrons collide with the specimen atom's own electrons, knocking some of them out of bound states. A vacant position in an inner-shell orbit is eventually occupied by a higher energy electron from an outer shell, which, meanwhile, gives up some of its energy by emitting an x-ray quantum. The amount of energy released during this process depends solely on the atomic type. An EDX spectrum normally does not depend on the atom's valence bond, since most of the x-rays are generated by electron transfer within inner shells (figure 4). By measuring the wavelengths of energy present in the x-rays being released by a specimen during electron-beam bombardment, the identity of the atoms in the sample can be determined.

The x-rays are generated from the sample surface up to 2  $\mu\text{m}$  in depth, depending on the energy of the electron beam and the material of the specimen, [13] and thus EDX is not a true surface sensitive technique. An EDX spectrum normally displays peaks corresponding to the energy levels for which the most x-rays have been received. As shown in Figure 5.3, normally  $K\alpha$ ,  $K\beta$ ,  $K\gamma$ ,  $L\alpha$ ,  $L\beta$  and  $M\alpha$  transitions can be observed.



**Fig 4: left: EDX geometry; right: emission lines arising from transitions between electron energy levels of an atom.**

X-ray powder diffraction (XRD) is a rapid analytical technique primarily used for phase identification of a crystalline material and can provide information on unit cell dimensions. For crystalline materials, the interplanar spacing of an array of atomic planes can be calculated from the Bragg equation:

$$2d\sin\theta = \lambda$$

Where,  $\theta$  is half of the angle between the incident and diffracted beams, and  $\lambda$  is the wavelength of the x-ray radiation.

### 2.1.5 X-Ray Reflectometry (XRR)

The operation mode of grazing-angle incidence x-ray reflectivity (XRR) is the  $\theta$ - $2\theta$  geometry, similar to the arrangement shown in Figure 5, but the intensity of the monochromatic x-ray beam reflected by a sample is recorded at grazing angles. Since the refractive index of x-rays in all materials is slightly less than 1, a beam in air impinging on a flat surface will be totally reflected at a critical angle  $\theta_c$ , and this critical angle for total reflection is extremely small. For most materials it can only be observed at grazing angles of incidence below  $0.3^\circ$ . Above  $\theta_c$  the reflections from layer interfaces interfere with each other and lead to interference fringes, which can be analyzed using the classical theory (Fresnel equations). Using mathematical models, the film density can be determined from the value of  $\theta_c$ , and the period and intensity of reflection fringes are related to the thickness and the roughness of the layer. At even larger angles, the reflectivity decreases very rapidly due to strong absorption of x-rays during increasing penetration into the material, therefore, the typical range for XRR measurements is  $0^\circ < \theta < 4^\circ$ .

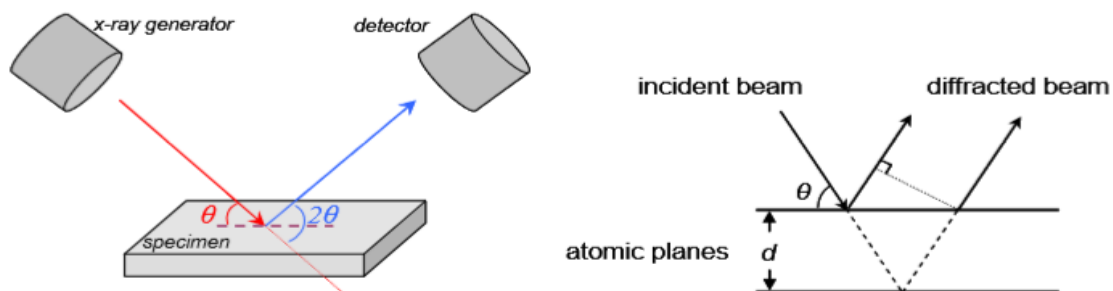


**Fig 5: left: XRD geometry; right: Bragg condition.**



### 2.1.6 Ellipsometry

Reflection ellipsometry is one of the methods used to characterize the thickness of the oxide thin films grown by ALD. A HeNe laser source (632.8 nm) is used to generate a light beam, which passes through a linear polarizer before being reflected from the thin film surface. The polarized light has two sinusoidally oscillating components: a *p* component parallel to the plane of incidence and an *s* component perpendicular to the plane of incidence. When the linearly polarized light reflects from a medium with a certain refractive index, the *p* and *s* components undergo different phase shifts; therefore, after the reflection, the beam is normally elliptically polarized, and detected by a photomultiplier. The two components of reflectivity are written as *r<sub>p</sub>* and *r<sub>s</sub>*, and ellipsometry measures the complex reflection coefficient ( $\kappa$ ), which is the ratio of *r<sub>p</sub>* and *r<sub>s</sub>*:

$$\kappa = \frac{r_p}{r_s} = \tan \psi e^{i\Delta}$$

in which  $\tan(\psi)$  is the amplitude ratio upon reflection, and  $\Delta$  is the phase shift. Ellipsometry does not directly measure the parameters of the sample; rather, a model analysis must be performed in order to derive the optical constants and thickness parameters of the sample from the calculated  $\psi$  and  $\Delta$  values.

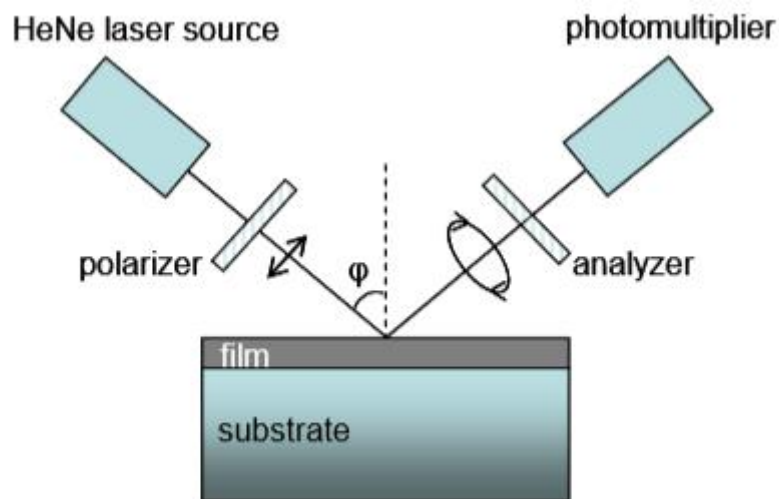


**Fig 6: Experimental arrangement in ellipsometry.**

### 2.1.7 Vibrating Sample Magnetometer (VSM)

The VSM is schematically shown in Fig 7. In this instrument the magnetic field is controlled by an electromagnet. This magnetic field magnetizes the sample, which is vibrated up and down at a relatively high frequency. The magnetized sample creates a flux in the pick-up coils, where a voltage is induced due to changes of flux caused by the sample vibration. The applied magnetic field could be varied between 0 and 1.9 T, and the sensitivity is  $10^{-6}$  emu. All measurements were performed under ambient conditions.

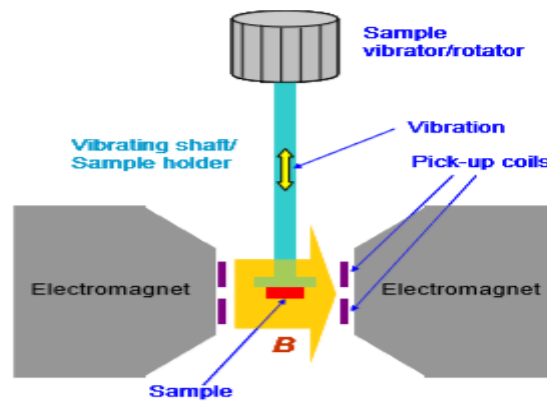


Fig 7 : Sketch of a VSM.

### 2.1.8 SQUID Magnetometry

The superconducting quantum interference device (SQUID) is regarded as one of the most sensitive magnetometers used to measure extremely weak magnetic fields with very high resolution and accuracy. The basic setup of a SQUID is similar to that of a VSM but with a combination of superconducting loops and Josephson junctions, as shown in Fig 8.

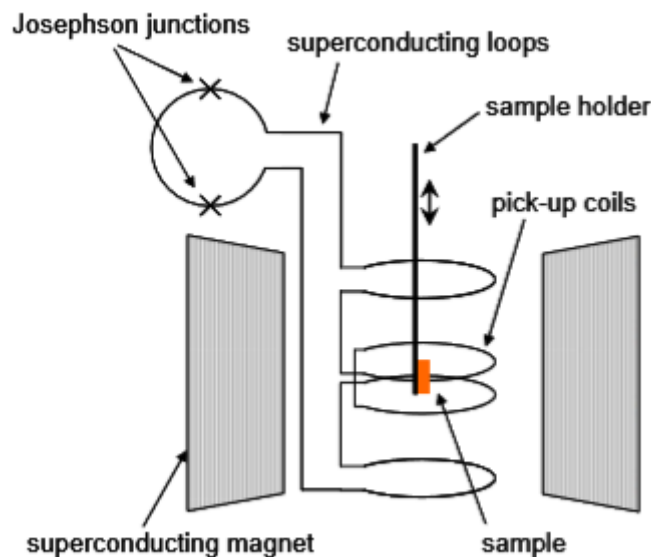


Fig 8: Schematic of a SQUID.

### 2.1.9 Piezoelectric-Membrane Axial Vibrator (PMAV)

Recently, a new device named “piezoelectric-membrane axial vibrator” (PMAV) was developed to measure the rheological properties of magnetic fluids. The general theory of the working principle of the PMAV—“squeeze flow”.

The PMAV, consisting of a pair of yokes, is attached to a rigid base and surrounded by a magnetic coil, as shown in Fig 9. The gap between the yokes can be adjusted from about 50 μm to the millimeter range by adding thin stainless steel spacer foils of well-defined thickness. The narrow gap is designed for the characterization of sample volumes as small as 50 μl. The sample is placed in the air gap between the cores of the yokes, which are

covered by smooth thin glass plates ( $\phi = 20$  mm). The lower plate that holds the sample is connected to eight piezoelements. The motion of the piezoelements is controlled by a programmable lock-in amplifier. Four of the elements are used to generate the excitation signal of desired frequency (8 to 200 Hz); thus, the lower plate can oscillate at this frequency with approximately 5 nm amplitude in the vertical direction. The liquid sample in the gap will experience a squeeze flow. The other four piezoelements act as sensors, which detect the response of the system and feed it back to the read-out ports of the lock-in amplifier. By means of an electromagnetic coil, the sample can be subjected to axial magnetic fields as strong as 110 mT. The temperature of the sample is controlled by a thermostat at  $20^{\circ}\text{C} \pm 0.3^{\circ}\text{C}$ , and an airtight compartment was constructed to enclose the PMAV measuring system in order to prevent water from condensing on the system and spoiling the sample. The reproducibility of the viscosity measurements made with this apparatus was found to be better than 0.3 mPa.s.

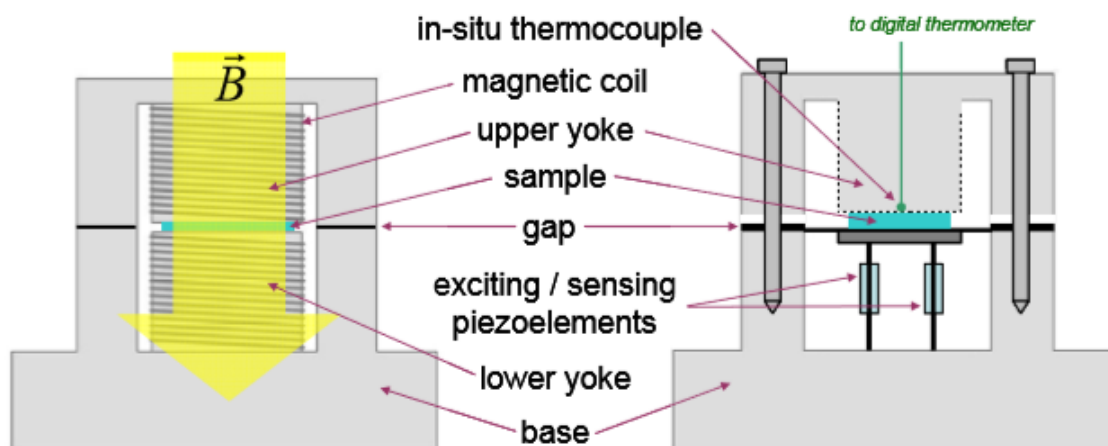


**Fig 9: Sketch of the PMAV with its axially vibrating piezoelements and gap between two flat surfaces, which establish the squeeze flow.**

### III. CONCLUSION

This Paper deals with the techniques applied to small tubular structures in order to evaluate their properties. The diversity and the fabulous potential of applications of the nanostructures is briefly reviewed by presenting some advances in nanotechnologies. Then, these techniques help to evaluate the behavior of tubular nanostructures. From the information delivered by these methods, the morphology, elemental composition, phase transitions, crystallinity, optical properties and magnetic properties of the samples can be determined. For many fields of the nanotechnologies, we are more observers than actors, still being surprised by the ability of the nature in synthesizing fine and elegant nanostructures in ambient temperature, while we have to use high pressure and/or high temperature. Nevertheless, the tendency is gently changing.

### IV. FUTURE ASPECTS

The future developments at an industrial level of Nano-objects with specific physical and chemical properties chosen in function of their applications will probably have a strong economic and social impact on the human being, notably for diseases treatments where nanotechnologies already afford novel techniques such as the



intracellular imaging through attachment of quantum dots or synthetic chromophores to selected molecules. Although wide benefits emerge from the nanotechnologies, we have also to keep in mind that the toxicology of many nanomaterials has not yet been fully evaluated. Thus, while nanotechnology promises many solutions related to health care or energy saving based for example on low weight high strength materials, it remains important to develop at the same time the knowledge of their impact on our environment and for this, it is important to characterize as accurately as possible each nanomaterial.

## REFERENCES

- [1]. C.-C. You, O. R. Miranda, B. Gider, P. S. Ghosh, I.-B. Kim, B. Erdogan, S. A. Krovi, U. H. F. Bunz, and V. M. Rotello, *Nat. Nanotech.* 2, 318 (2007).
- [2]. H. W. Kroto, J. R. Heath, S. C. O'Brien, R. F. Curl, and R. E. Smalley, *Nature* 318, 162 (1985).
- [3]. S. Iijima, *Nature* 354, 56 (1991).
- [4]. H. Dai, E. W. Wong, Y. Z. Lu, S. Fan, and C. M. Lieber, *Nature* 375, 769 (1995).
- [5]. W. Q. Han, S. S. Fan, Q. Q. Li, B. L. Gu, X. B. Zhang, and D. P. Yu, *Appl. Phys. Lett.* 71, 2271 (1997).
- [6]. P. D. Yang and C. M. Lieber, *J. Mat. Res.* 12, 2981 (1997).
- [7]. Y. Li, G. S. Cheng, and L. D. Zhang, *J. Mat. Res.* 15, 2305 (2000).
- [8]. M. Knez, A. Kadri, C. Wege, U. Glosele, H. Jeske, and K. Nielsch, *Nano Lett.* 6, 1172 (2006).
- [9]. A. Dodabalapur, H. E. Katz, L. Torsi, and R. C. Haddon, *Science* 269, 1560 (1995).
- [10]. K. K. W. Wong, T. Douglas, S. Gider, D. D. Awschalom, and S. Mann, *Chem. Mater.* 10, 279 (1998).
- [11]. D. B. Williams and C. B. Carter. *Transmission electron microscopy: a textbook for materials science.* (Plenum Press, 1996).
- [12]. C. Kübel, A. Voigt, R. Schoenmakers, M. Otten et al. Recent advances in electron tomography: TEM and HAADF-STEM tomography for materials science and semiconductor applications. *Microscopy and Microanalysis* 11 (2005), 378-400.
- [13]. J. Goldstein, D. E. Newbury, D. C. Joy, C. E. Lyman et al. *Scanning Electron Microscopy and X-Ray Microanalysis.* (Springer, 2003).